Volume 1 | Number 1 | Jan 2013 | Pages 1–100

Journal of
Materials Chemistry A

Materials for energy and sustainability
www.rsc.org/materialsA

Li⁺

ROYAL SOCIETY
OF CHEMISTRY

ROYAL SOCIETY
OF **CHEMISTRY**

www.rsc.org/materialsA

Electrochemically generated sol-gel films as the inhibitor containers of superhydrophobic surface for active corrosion protection of metals

Xue-Fen Zhang, Rui-Jiao Chen, Yan-Hua Liu and Ji-Ming Hu*

The present work shows a new contribution to the design of superhydrophobic surface with an additional function of active corrosion protection, by the encapsulation of inhibiting agents. Superhydrophobic silica films are fabricated on aluminum alloy using electro-assisted deposition from sol-gel precursors. Two kinds of inhibitors, either the inorganic cerium nitrate or organic benzotriazole, are incorporated into the superhydrophobic films by two-step or one-step route. The corrosion protection performance is investigated by electrochemical impedance spectroscopy and scanning vibrating electrode technique, as well as by monitoring changes of the water contact angle. The results reveal that the superhydrophobic films loaded with inhibitors show a greatly improved anticorrosion property in 3.5 wt. % NaCl aqueous solution.

1 Introduction

One of the biggest obstacles for the usage of metals and their alloys is the high susceptibility to corrosion attack when exposed to ambient environment, which causes numerous economic loss and potential safety hazards [1]. Much effort has been made to reduce the corrosion rate of metals, especially for those used in aggressively corrosive media containing chlorine anion. Conventionally, phosphating or chromating-based processes are two commonly used strategies for corrosion inhibition of metals. Though the satisfied anticorrosion performance, these processes are facing the predicament that they are grimly forbidden in many countries due to the notorious water eutrophication caused by phosphate compounds and carcinogenic effects to human due to the high toxicity of chromium (VI) [1, 2]. Up to now, variously alternative protection methods have been developed to address the above problem, such as sol-gel derived film [2-5], rare-earth salt conversion layer [6-8], conducting polymeric films [9-11], etc.

Recently, superhydrophobic surface, with water contact angle (CA) larger than 150 º and sliding angle (SA) less than 10 º by definition, has attracted tremendous attention in the fields of surface engineering [12-15]. Materials with such special wettability can act as effective physical barrier in aqueous environment. The good barrier property is believed to be a result of highly rough and porous morphology existing in the superhydrophobic materials, which has the ability to entrap large amount of air [16]. For this reason, superhydrophobic films have recently found their new application in corrosion protection of metallic substrates, such as steels, copper, zinc, magnesium and aluminum and their alloy [16-26].

Nevertheless, the physical barrier of superhydrophobic materials can only provide passive corrosion protection. They often cannot meet the requirement of long-term utilization. In this case, active corrosion protection is desired, aiming at a decrease of the corrosion rate when the barrier layer is damaged and the corrosive species arrive at the substrate. Very often, the active protection of metals is provided by introducing corrosion inhibitors. To the best of our knowledge, however, corrosion inhibitors have never been introduced into superhydrophobic barriers to fabricate protection system with the combined functions of both passive and active corrosion protection.

Corrosion inhibitors can be incorporated into the protection system by different ways. One of the most commonly used methods is the direct addition of inhibitors in the pretreatment, primer or topcoat [27, 28]. However, a too high concentration or low solubility of the inhibitors often results in a deterioration of integrity and physical barrier properties of the matrix of protection system [29]. In addition, the existing interaction of the inhibiting agents with the protective matrix often leads to significantly reduced stability of protective layer and the deactivation of the inhibitors [30]. Another newly emerged method for inhibitor incorporation is the pre-encapsulation by nanoparticles container, preventing the direct interaction of inhibitor with the protection matrix (i.e. pretreatment, primer or topcoat layers) and controlling its release [31]. Due to the high pore volume and surface area, mesoporous silica nanoparticles were reported as the

Department of Chemistry, Zhejiang University, Hangzhou 310027, China. E-mail: kejmhu@zju.edu.cn

promising nanocontainers for the construction of active anti-corrosive coating system [28]. The anticorrosive sol-gel coatings doped with inhibitor-loaded silica nanocarriers show enhanced corrosion protection for aluminum alloy and carbon steels [30, 32-35].

One could look back the physicochemical characteristic of superhydrophobic surface, that is the combination of high roughness and low surface energy [36, 37]. The highly rough and porous microstructures might allow for the corrosion inhibitor storage with desired amount in the porous matrix. On the basis of this demonstration, in this work, an enhanced corrosion protection for metals by superhydrophobic sol-gel films loaded with two different kinds of inhibiting agents is presented. As the successor of our recent publications, the superhydrophobic surface is fabricated on electrochemically generated silica (E-SiO$_2$) films by either two-step [38] or one-step route [39]. Compared with conventional dip-coating technique, the electro-assisted process ensures their higher roughness and porosity of the generated sol-gel films [40, 41], and therefore meets the requirement of superhydrophobicity. Preliminary experiments showed that superhydrophobic sol-gel films prepared by one-step electrodeposition provide corrosion protection for mild steel [12].

2 Experimental Section

Materials and chemicals

Commercially available aluminum alloy AA2024-T3 plates with the size of 2.0 cm × 4.0 cm (0.1 cm thick) were used as the model metallic substrates. Prior to use, the substrates were abraded consecutively with finer emery papers to 400 grade, followed by ultrasonically rinsed with ethanol and deionized (DI) water for 10 minutes, respectively. Then the substrates were dried with blowing nitrogen and sealed with insulation paster on one side to leave an exposure area of 2.0 cm × 2.0 cm on the opposite side. Sodium nitrate (NaNO$_3$, ≥ 99.0 %), cerium (III) nitrate hexahydrate (Ce(NO$_3$)$_3$·6H$_2$O, ≥ 99.0 %), potassium hydroxide (KOH), sodium hydroxide (NaOH), ethylene diamine tetraacetic acid disodium salt (EDTA, ≥ 99.0 %), xylenol orange (≥ 75.0 %), hydroxylammonium chloride (NH$_2$OH·HCl, ≥ 98.5 %), acetic acid (HAc, ≥ 98.5 %), and absolute alcohol (EtOH, > 99 %) were purchased from Sinopharm Chemical Reagent Co., Ltd. (China). Tetraethoxysilane (TEOS, > 99 %) and 1H-benzotriazole (BTA, 99%) were provided by Aladdin Industrial Corporation (China). Dodecyltrimethoxysilane (DTMS, > 93 %) was provided by Tokyo Chemical Industry Co., Ltd. (Japan). All the chemical reagents were used without further purification.

Preparation of superhydrophobic surfaces

Two-step or one-step route was used for the preparation of superhydrophobic sol-gel silica films. The experimental details can be individually found in our previous work [38, 39].

In a two-step method, highly porous SiO$_2$ films were firstly electrodeposited onto aluminum alloy substrate from a precursor solution consisting of 50 mL EtOH, 50 mL 0.2 M NaNO$_3$ and 5 mL TEOS (pH 4.5, adjusted with HAc). The deposition was conducted at -1.5 V (vs. Ag/AgCl electrode in saturated KCl solution) for 300 s in a three-electrode cell, followed by rinsing with DI water and ethanol consecutively and finally dried in an oven at 40 °C for 6 h. The low surface energy was achieved in the second step by immersing the silica films into a pre-hydrolyzed DTMS solution consisting of 80 mL EtOH, 20 mL H$_2$O and 5 mL DTMS (pH 4.5, adjusted with HAc). In order to load inhibiting agent of Ce(NO$_3$)$_3$, prior to DTMS modification, the silica films were immersed in 100 mL DI water containing 0.685 g Ce(NO$_3$)$_3$·6H$_2$O and 0.68 mL H$_2$O$_2$ at 35 °C for 5 min, followed by drying at 100 °C for 1 h to fully solidify the inhibitor-loaded silica films.

For encapsulating BTA inhibitor, the superhydrophobic films were generated by one-step from a hybrid precursor solution (pH 4.5, adjusted with HAc) consisting of 80 mL EtOH, 20 mL 0.2 M NaNO$_3$, 2 mL TEOS, 2 mL DTMS and 0.1 g (~ 1.0 g/L) BTA by the electrodeposition at -1.5 V vs. Ag/AgCl for 300 s. For comparison, superhydrophobic films were also prepared from the similar precursor but without BTA. After electrodeposition, the samples were rinsed with DI water and EtOH, respectively, finally dried in an oven at 40 °C for 6 h.

A schematic description for encapsulating the above-mentioned inorganic or organic inhibitor is depicted in Fig. 1.

Characterization and analysis

The morphology observation of the superhydrophobic surfaces was carried out by scanning electron microscopy (SEM, SU8010, HITACHI, Japan) with an 3.0 kV operating voltage equipped with energy dispersive spectrometer (EDS, IXIF systems). The water contact angle was measured on a JC2000D
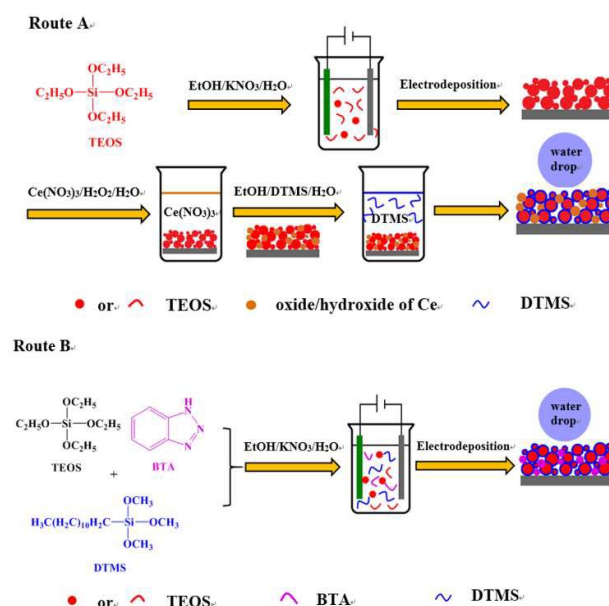

Fig. 1 Schematic illustration of the fabrication of superhydrophobic film containing inorganic cerium salt compound (route A) and organic BTA (route B) with active corrosion protecting property.

contact angle instrument (Shanghai Zhongchen Digital Technic Apparatus Co. Ltd. China). A 5 µL water drop was dropped carefully onto the samples and the final CA values were determined by averaging the measured data at five randomly selected positions at ambient temperature (25 °C). Film thickness was measured by a profilometer (Dektak 150, Veeco, USA). A notch was made artificially by using a wooden stick.

The chemical compositions of the inhibitor-contained superhydrophobic film were studied by X-ray photoelectron spectroscopy (XPS, ESCALAB 250Xi, thermo scientific, England) using Al Kα radiation (1486.6 eV, 180 W) as the excitation source. For the purpose of depth profiling, the spectra were collected after sputtering by Ar$^+$ ion with 3 kV and 10 mA at a certain time interval. The binding energy of carbon (C1s: 285 eV) was used as the reference.

The loading capacity of cerium in the electrodepsited silica films was determined using EDTA complexomentry. 10 wt. % NH$_2$OH·HCl was added into the cerium solution, which is used for inhibitor encapsulation of silica films, to reduce the Ce (IV) to Ce (III). 0.02 M EDTA was introduced to act as chelating ligands with 0.5 wt. % xylenol orange used as the indicator. The final cerium loading is a measure of cerium consumption in the cerium solution, as calculated by concentration subtraction before and after loading process by fresh silica films samples.

The loading capacity of BTA in hybrid films was quantitatively determined on an ultraviolet and visible (UV-Vis) spectroscopy (UV-2550, SHIMADZU, Japan) in an EtOH solvent after entire releasing of BTA from the artificially scratched silica powders and 259 nm was used as absorbance wave

Corrosion performance evaluation

Electrochemical impedance spectroscopy (EIS) was performed on a M273 model potentiostat (Princeton Applied Research, USA) combined with a M5210 model lock-in amplifier (Signal Recovery, USA) in a classical three-electrode cell filled with 3.5 wt. % NaCl aqueous solution. A Pt plate and Ag/AgCl (in the saturated KCl solution) were used as the counter and reference electrodes, respectively. The experiments were operated at open-circuit potential (OCP) in the frequency range from 100 kHz to 10 mHz by applying an AC excitation amplitude of 10 mV (peak to zero) sinusoidal voltage. Before measurements, the edge area and the back side of the superhydrophobic film-coated samples were sealed with epoxy resin to neglect the un-uniformity. Prior to measurement, the samples were immersed in the testing solution for 0.5 h.

The scanning vibrating electrode technique (SVET, Versascan, AMETEK, USA) was used to evaluate the local corrosion behaviour of the superhydrophobic samples in 0.1 M NaCl solution. The vibrating electrode was made of platinum-iridium covered with polymer, leaving only an uncovered tip with a diameter of ~ 10 µm. The distance of the tip to the surface was kept at 100 µm and the scanned area was 2.0 mm × 2.0 mm. The vibration frequency was set to 80 Hz, and the peak-to-peak amplitude was 30 µm. Before measurements, a scratch with ~1 mm length and 200 µm width was made artificially on the surface of superhydrophobic film-coated substrates using a surgical knife to ensure the exposure of the metal to the corrosive solution.

3 Result and discussion

SEM images of aluminum alloy after various treatments are summarized in Fig. 2. As shown in Fig. 2a, the electrodeposited SiO$_2$ films are composed of a large number of unconnected flower-shaped micro/nanostructure and a few of cracks. This special structure is attributed to the accumulation of spherical silica particles. The water droplet (5 µL) completely spreads on the SiO$_2$-coated substrate with CA value of 0 °, indicating the superhydrophilicity of SiO$_2$. After modification with low surface energy compound (DTMS) (Fig. 2b), less changes occur in microtopography and the CAs increase to 157.6 ± 1.8 ° (SA = 3.3 ± 1.7 °), indicating that superhydrophobic surface can be constructed on the porous silica matrix. After treated with cerium, the color of the thin film changes from white to light yellow and the flower-shaped microstructure is connected with each other by sheet structure with less cracks (Fig. 2c). The substrate wettability changes from superhydrophilic to hydrophilic with CA increasing from 0 ° to 53.1 ± 1.5 °, due to the morphology changes with less cracks induced by the generation of oxide/hydroxide of Ce. After the modification of DTMS, the water droplet stands as almost round shape with the CA of 158.1 ± 0.7 ° (SA = 3.3 ± 0.5 °), indicating that superhydrophobic film loaded with Ce compound inhibitor is successfully prepared (Fig. 2d).
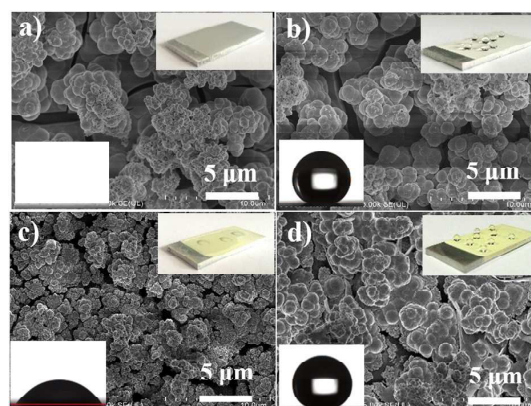

Fig. 2 SEM images of electrodeposited SiO$_2$ films (a, b) and Ce-entrapped SiO$_2$ film (c, d) before (a, c) and after (b, d) DTMS modification. The insets display the water droplet on the surface.

The chemical composition of cerium salt-encapsulated SiO_2 films is further analyzed by EDS and XPS. Strong EDS signals of O, Si and Ce elements can be observed (Fig. 3a). The detection of Zr is mainly due to the existence of small amount of such impurity in commercially provided $Ce(NO_3)_3 \cdot 6H_2O$. The abundance of Ce in porous silica is noticed by comparing the elements mapping of Si and Ce (Figs. 3b and 3c). The element mapping result clearly shows that the inhibiting agents mainly occupy in the boundaries of silica spherical particles. The concentrations of elements existing in the hybrid silica films are listed in Table S1. The Ce/Si/O atomic ratio is about 1: 5.22: 10.39 and the corresponding weight percentage of $Ce(NO_3)_3 \cdot 6H_2O$ is ~ 58 wt. % of silica, which is in good agreement with the results detected by EDTA complex titrimetry (~ 59 wt. %).

XPS detection also shows strong signals of Si 2p, O 1s, C 1s and Ce 3d (Fig. S1a). High resolution of Ce 3d spectra gives ten peaks in the binding energy range from 930 eV to 870 eV (Fig. S1b), which can be divided into five doublets corresponding to $3d_{5/2}$ and $3d_{3/2}$. Among the 5 doublets, three doublets labelled as v-u (883.7 eV and 901.7 eV), v''-u'' (888.7 eV and 908.0 eV) and v'''-u''' (898.9 eV and 917.7 eV) are attributed to the presence of Ce (IV), and the other two doublets, v_0-u_0 (882.4 eV and 900.2 eV) and v'-u' (886.2 eV and 904.5 eV) are due to the existence of Ce (III) [42-44]. According to the above results and previous reports [42, 45-48], we can conclude that cerium compound entrapped in the silica film exists in the form of oxides/hydroxides of Ce (III) and Ce (IV). The XPS in depth shows that oxides/hydroxides of Ce (III) or Ce (IV) disperse not only at the surface but also in the bulk of silica film (Fig. S1c). If taking into account the total sputtering time (5×10^4 s) in the depth profile of Ce element, the effective depth of cerium conversion layer would be as deep as 1 μm (~ 1.2 nm/min of sputtering rate), which can explain the relatively high weight percentage of the inhibitor in the silica films.

Superhydrophobic films are commonly used in moderate environment. However, in order to shorten the testing time, aggressively corrosive NaCl solution is used in this research as the testing solution for corrosion performance evaluation. Bode plots (Fig. 4a) show that superhydrophobic surfaces (curve 2, 3), irrespective of cerium compound incorporation,
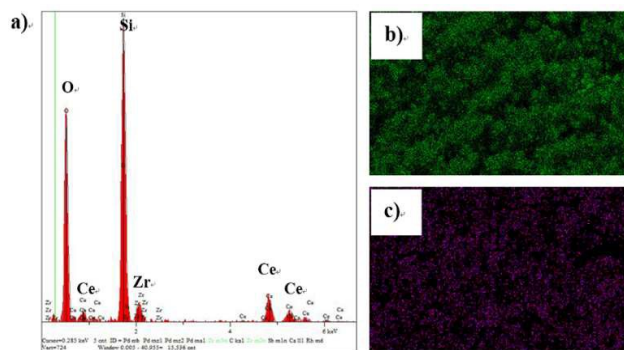

Fig. 3 The EDS spectra (a) and elements mapping of Si (b) and Ce (c) in Ce-incoporated superhydrophobic silica film coated on the Al alloy.
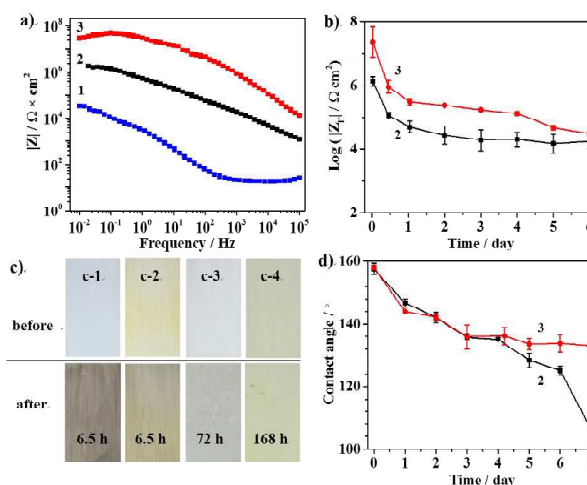

Fig. 4 Bode plots after immersion for 0.5 h (a) and evolution with immersion time of low-frequency impedance (b) (measured at 0.10 Hz) in 3.5 wt. % NaCl solution of bare (1), superhydrophobic silica (2) and Ce-incorporated superhydrophibic silica (3) film-coated electrodes. (c) Optical images of bare silica (c-1), Ce-incorporated silica (c-2), superhydrophobic silica (c-3), superhydrophobic Ce-incorporated silica (c-4) films-coated Al alloy before (upper) and after (bottom) immersion in 3.5 wt. % NaCl solution for different times. (d) Change of water CAs of the superhydrophobic silica (2) and Ce-contained superhydrophibic silica (3) film-coated samples over time of the immersion in 3.5 wt. % NaCl solution.

exhibit obviously higher impedance and therefore provide significantly improved corrosion resistance to the bare aluminum alloy substrate (curve 1). The encapsulation of cerium inhibitor further increases the impedance values (~ 1 order of magnitude higher at low frequency) of superhydrophobic silica films, indicating the additional corrosion inhibition effect of the entrapped cerium compound. The evolution of low frequency impedance modulus ($|Z_{lf}|$ at 0.1 Hz) suggests that the cerium-contained films maintain their pronouncedly improved protectiveness over a long time's immersion (within 6 days) in 3.5 wt. % NaCl solution (Fig. 4b).

Optical images directly differentiate the anticorrosion properties of differently filmed samples (Fig. 4c). Corrosive destruction of aluminum alloy covered with electrodeposited silica-alone is clearly observed after immersion in NaCl solution for only 6.5 h (Fig. 4c-1). At this time, no obvious corrosive destruction is observed on cerium-loaded silica films (Fig. 4c-2). As expected, the superhydrophobic surfaces achieved after low energy modification provide enhanced protectiveness (Figs. 4c-3, 4c-4). Nevertheless, after immersion for 72 h, corrosion products appear on the surface of superhydrophobic silica films (Fig. 4c-3), while the Ce-incorporated film prolongs their immersion time for corrosion initiation to 168 h (Fig. 4c-4). Meanwhile, CA monitoring shows that both the two surfaces consecutively lose their superhydrophobicities during the first day's immersion due to the surface changes caused by corrosive media attacking (Fig.

ARTICLE

4d). The superhydrophobic surface constructed on silica film-alone continuously decreases in its hydrophobicity for further immersion. Contact angle of superhydrophobic surface fabricated on Ce-contained silica films, however, remains almost unchanged after this time (3 days). The different change tendency of CA is believed as a result of different corrosion activities of aluminum alloy substrates covered with individually anticorrosive films.

The corrosion process naturally causes local fluxes of cations and anions, which can be detected by the vibrating electrode moving above the surface of substrates. Fig. 5 depicts the current maps obtained by SVET measurements in 0.1 M NaCl solution on the Al alloy coated with the superhydrophobic silica film before (Fig. 5a) and after the encapsulation of cerium compound (Fig. 5b). For substrates protected by the superhydrophobic silica film-alone, a pitting corrosion site can be detected at the initial immersion time in the scratched area (left in Fig. 5a). After 12 h of immersion, the corrosion area expands and the anodic current density increases dramatically (middle in Fig. 5a). This phenomenon is predictable since the barrier performance of non-active silica matrix is destroyed after defect formation. In contrast, incorporation of cerium compound in superhydrophobic film leads to a distinct decrease of anodic current densities and the suppression of development of corrosion process during the immersion in NaCl solution (Fig. 5b). Such a big distinction between these two superhydrophobic films can be more clearly seen from the evolution of anodic current over the immersion time (right in Fig. 5). The improved anticorrosive performance is contributed to the deposition of oxide/hydroxide of cerium at the cathodic site due to the local pH increase when corrosion occurs, which effectively blocks the cathodic reaction and hinders the whole corrosion process [43].

Benzotriazole (BTA), another often used organic inhibitor [11, 45], is also tried in this work to demonstrate the wide versatility of inhibitor encapsulation in superhydrophobic surface. This inhibiting agent works in different mechanism compared with cerium salt compound. The former plays an adsorption role and the latter presents inhibiting effect via precipitation mechanism [43, 44, 49]. The UV-Vis absorbance of SiO_2 films after immersed for 300 s in BTA/EtOH solution increases rapidly with increasing the concentration of BTA in the adsorption solution up to 10 g/L of BTA concentration, after which saturated adsorption of BTA is achieved (Fig. S2a). The loading of BTA, as determined by the concentration subtraction calculated from the different UV-vis absorbance intensity of BTA/EtOH solution before and after adsorption by silica film, is ~ 285 mg(BTA) /1 g(SiO_2). This value is slightly lower than that of mesoporous silica nanoparticles (409 mg(BTA)/1 g(SiO_2)), as reported by literature [29]. Nevertheless, the comparable loading capacity with mesoporous container suggests the highly porous microstructure of electrodeposited silica films.
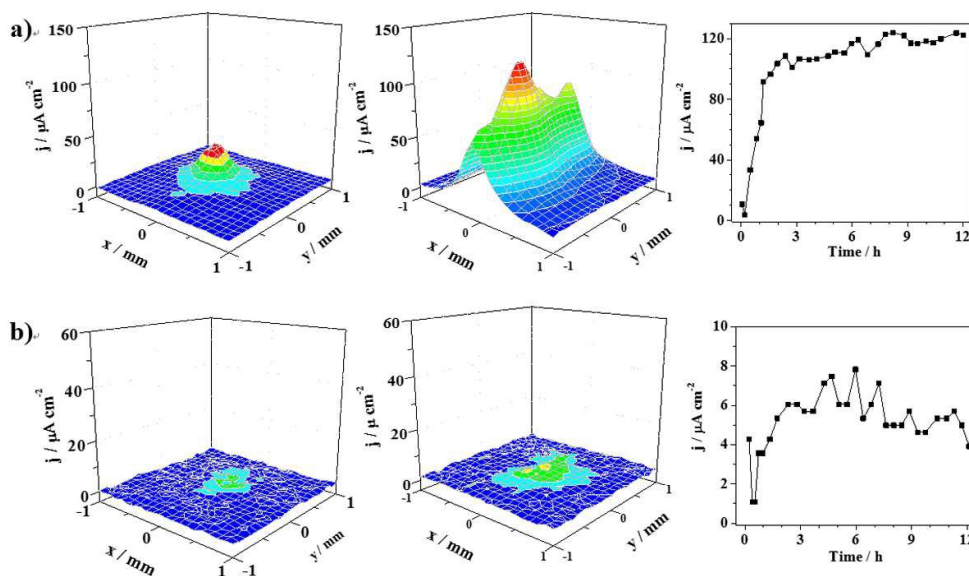

Fig. 5 Left and Middle: SVET current density maps of Al alloy substrates coated with superhydrophobic silica (a) and Ce-incorporated superhydrophobic silica films (b) after immersion in 0.1 M NaCl solution for 0.5 h (left) and 12 h (middle). Right: Maximum anodic current densities versus immersion time in 0.1 M NaCl solution.

However, the major problem of such two-step method is the great extent of dissolution of organic inhibitor into the following low-energy modifying precursor (DTMS/EtOH/H$_2$O). UV-Vis spectroscopy test shows that the BTA signal of silica films pre-adsorbed in 10 g/L BTA solution totally disappears after immersed in DTMS solution for 300 s (Fig. S2b). EIS measurement indicates that no improvement in corrosion performance is obtained for two-step BTA-entrapped films (data not shown). To overcome this problem, one-step approach is proposed for BTA incorporation in superhydrophobic silica film system. The hybrid superhydrophobic films are simply electrodeposited from a mixed precursor containing TEOS, DTMS and BTA (Fig. 1b). The existence of BTA in the precursor is found having no significant effect on the electrodeposition kinetics of the hybrid films (Fig. S3). However, the superhydrophobicity is lost when the concentration of BTA increases to 2.0 g · L^{-1} (Fig. S3). To ensure the superhydrophobic property, the concentration of BTA in the precursor is controlled as 1.0 g/L in this work. The SAs of the above-prepared hybrid superhydrophobic film before and after BTA entrapment are 5.5 ± 0.7 °, 5.6 ± 0.7 ° respectively. As measured by UV-Vis spectroscopy, the loading capacity of BTA in this hybrid film is ~ 25 mg(BTA)/1 g(SiO$_2$), a value nearly one tenth of that in E-SiO$_2$ films after dipping into BTA/EtOH (10 g/L) solution via two-step method (285 mg(BTA)/1 g(SiO$_2$)) as mentioned above. This value is far smaller than that of cerium compound (58-59 % as mentioned before). Such a big difference is reasonable because the former is loaded by adsorption and the latter is entrapped by precipitation.

The release kinetics of BTA from the superhydrophobic films is further investigated in aqueous solutions with different pH. Noticing that such one-step films, irrespective of BTA incorporation, are superhydrophobic in aqueous solution with wide pH range (see contact angle values, Fig. 6a). Fig. 6b shows that the inhibiting agent releases rapidly at the initial immersion stage, followed by gradually decreased leaching. Compared with the neutral solution, either acidic or basic condition facilitates the BTA releasing from superhydrophobic silica matrix. This phenomenon is probably caused by the larger electrostatic repulsion forces between the silica particles and the inhibitor molecules which have the same charge at pH values different from neutral [29]. As corrosion process is always followed by alkaline or acidic pH shift in the solution near the metallic substrate, the fast release of BTA inhibitor at either acid or basic condition is favorable for the use of silica containers in active anticorrosion coating.

EIS measurements in NaCl solution show that the low frequency impedance (at 0.1 Hz) of superhydrophobic silica films incorporated with BTA is 4 times higher than that of BTA-free specimen at the initial immersion time (Fig. 7a). Prolonging the immersion time results in bigger impedance difference in impedance value between these two samples, indicating that BTA acts as "self-healing" agent in accompany with the corrosion of metallic substrate during the immersion. The BTA encapsulation is found having no negative effect on
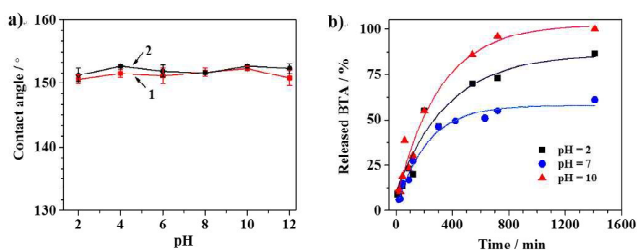

Fig. 6 (a) CA of hybrid superhydrophobic film before (1) and after (2) BTA entrapment in aqueous solution with different pH. (b) Release of BTA from porous hybrid superhydrophobic film in water solution with different pH values.
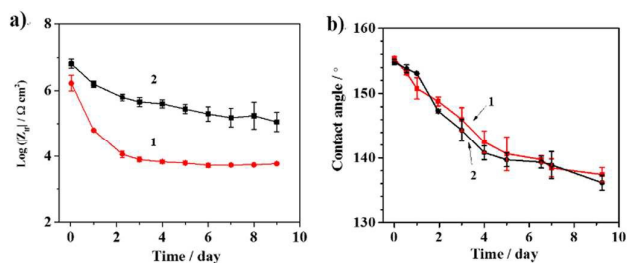

Fig. 7 Evolution with immersion time of low frequency impedance module (a, measured at 0.1 Hz) and change of water contact angle (b) of superhydrophobic film coated aluminum alloy before (1) and after (2) BTA entrapment.

hydrophobicity degradation during the aggressive immersion (Fig. 7b).

The corrosion performance of BTA-loaded superhydrophobic films is also evaluated by SVET. The anodic activity of BTA-free hybrid superhydrophobic film measured at the initial immersion time (0.5 h) can be observed near the scratch (left, Fig. 8a). After immersed for 12 h (middle, Fig. 8a), the anodic current significantly increases, accompanying with the expansion of defect area. In contrast, an obvious suppression of corrosion process for aluminum alloy coated with BTA-incorporated superhydrophobic film is found during the total immersion time (left and middle, Fig. 8b). In this hybrid silica film, much smaller anodic current density is detected. The evolution of the maximum anodic current density more clearly shows the distinction of localized corrosion activity of different samples (right, Fig. 8). As demonstrated above, either the increase or decrease of local pH, which is a common result of metal corrosion, induces the release of BTA in sufficient amount from the silica matrix. In other words, the corrosion inhibition role of BTA-encapsulated superhydrophobic film is induced by corrosion process itself. The suppression of anodic and cathodic activity on metal substrates is achieved when BTA forms a dense film on the surface [29, 50].

4 Conclusions

In this study, we have proposed a new concept to provide superhydrophobic surface with an active anticorrosive
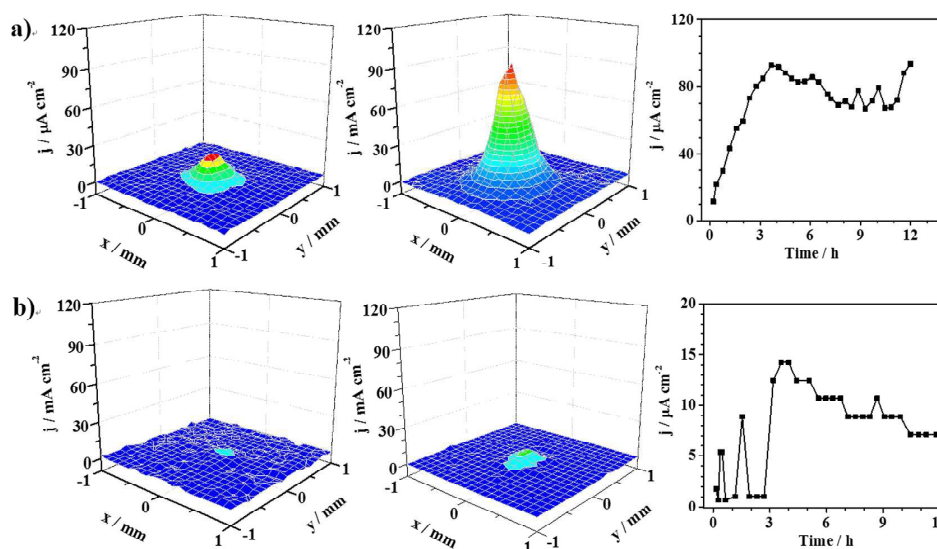
Fig. 8 Left and Middle: SVET maps of current density of BTA-free (a) and BTA-encapsulated (b) superhydrophobic films coated aluminum alloy after immersion in 0.1 M NaCl solution for 0.5 h (left) and 12 h (middle). Right: Maximun current densities versus time after immersion in 0.1 M NaCl solution.

property for metal substrates, by the incorporation of inhibiting agents. As the models, aluminum alloy and cerium salt compound and BTA are investigated as the substrate and inhibitors, respectively. Superhydrophobic surface used here is fabricated on the basis of electrodeposited silica films. The highly rough and porous structure, one of the required properties of superhydrophobic surface, allows for the loading of sufficient amount of corrosion inhibitor in the silica-based matrix. The successfully embedded either inorganic cerium salt or organic BTA in passive superhydrophobic silica films significantly improves the corrosion resistance of the aluminum alloy AA 2024-T3 in NaCl solution.

Different routes were employed to incorporate corrosion inhibitors with different chemical properties. Cerium salt forms oxide/hydroxide on silica surface in the presence of H_2O_2 via the precipitation process, therefore can be embedded into superhydrophobic films by two-step procedure. However, the organic inhibiting agents, e.g. BTA, are prone to leaching into the low-energy modifying precursor via the dissolution by organic solvent. Therefore, one-step electrodepostion was applied for the incorporation of BTA. Though the loading capacity of BTA in the one-step superhydrophobic films is much lower in comparison with that of cerium salt in two-step process, BTA-incorporated hybrid films still provide effective and active corrosion inhibition to aluminum alloy substrates. In this protection system, the pH-stimulated release of BTA indicates that the corrosion inhibition is triggered by the corrosion process itself.

The approach described here is a very general way for loading the corrosion inhibitors in superhydrophobic surface. It may be extended to other superhydrophobic films which are fabricated by different techniques, and also to long-term protection system (e.g. organic painting system [51], as firstly reported by our group) constructed on the electrodeposited

silica pretreatment layer. The attempt to load inhibiting agents at the latter protection system is in the progress in our laboratory and will be released in the near future.

References

1   L. K. Wu, L. Liu, J. Li, J. M. Hu, J. Q. Zhang and C. N. Cao, *Surf. Coat. Technol.*, 2010, **204**, 3920-3926.
2   L. L. Jiang, L. K. Wu, J. M. Hu, J. Q. Zhang and C. N. Cao, *Corros. Sci.*, 2012, **60**, 309-313.
3   S. A. S. Dias, S. V. Lamaka, C. A. Nogueira, T. C. Diamantino and M. G. S. Ferreira, *Corros. Sci.*, 2012, **62**, 153-162.
4   R. Akid, H. Wang, T. J. Smith, D. Greenfield and J. C. Earthman, *Adv. Funct. Mater.*, 2008, **18**, 203-211.
5   M. L. Zheludkevich, I. M. Salvado and M. G. S. Ferreira, *J. Mater. Chem.*, 2005, **15**, 5099-5111.
6   K. A. Yasakau, M. L. Zheludkevich, S. V. Lamaka and M. G. S. Ferreira, *J. Phys. Chem. B*, 2006, **110**, 5515-5528.
7   B. Davo and J. J. de Damborenea, *Electrochim. Acta*, 2004, **49**, 4957-4765.
8   W. Liu, F. Cao, L. Chang, Z. Zhang and J. Zhang, *Corros. Sci.*, 2009, **51**, 1334-1343.
9   J. E. P. da Silva, S. I. C. de Torresi and R. M. Torresi, *Corros. Sci.*, 2005, **47**, 811-822.
10 A. Kumar S, H. Bhandari, C. Sharma, F. Khatoon and S. K. Dhawan, *Polym. Int.*, 2013, **62**, 1192-1201.
11 L. Adamczyk and P. J. Kulesza, *Electrochim. Acta*, 2011, **56**, 3649-3655.
12 M. Qu, B. Zhang, S. Song, L, Chen, J. Zhang and X. Cao, *Adv. Funct. Mater.*, 2007, **17**, 593-596.
13 Y. Li, W. Cai, B. Cao, G. Duan, F. Sun, C. Li and L. Jia, *Nanotechnology*, 2006, **17**, 238-243.

14 Y. Li, G. Duan, G. Liu and W. Cai, *Chem. Soc. Rev.*, 2013, **42**, 3614-3627.

15 Y. Li, N. Koshizaki and W. Cai, Coordin. *Chem. Rev.*, 2011, **255**, 357-373.

16 L. K. Wu, X. F. Zhang and J. M. Hu, *Corros. Sci.*, 2014, **85**, 482-487.

17 Z. Wang, Q. Li, Z. She, F. Chen and L. Li, *J. Mater. Chem.*, 2012, **22**, 4097-4105.

18 R. Qiu, D. Zhang and P. Wang, *Corros. Sci.*, 2013, **66**, 350-359.

19 L. Zhao, Q. Liu, R. Gao, J. Wang, W. Yang and L. Liu, *Corros. Sci.*, 2014, **80**, 177-183.

20 J. Ou, W. Hu, M. Xue, F. Wang and W. Li, *ACS Appl. Mater. Interfaces*, 2013, **5**, 3101-3107.

21 Q. Liu, D. Chen and Z. Kang, *ACS Appl. Mater. Interfaces*, 2015, **7**, 1859-1867.

22 H. Liu, S. Szunerits, W. Xu and R. Boukherroub, *ACS Appl. Mater. Interfaces*, 2009, **1**, 1150-1153.

23 L. Li, T. Huang, J. Lei, J. He, L. Qu, P. Huang, W. Zhou, N. Li and F. Pan, *ACS Appl. Mater. Interfaces*, 2014, **7**, 1449-1457.

24 A. C. C. de Leon, R. B. Pernites and R. C. Advincula, *ACS Appl. Mater. Interfaces*, 2012, **4**, 3169-3176.

25 K. C. Chang, H. I. Lu, C. W. Peng, M. C. Lai, S. C. Hsu, M. H. Hsu, Y. K. Tsai, C. H. Chang, W. I. Hung, Y. Wei and J. M. Yeh, *ACS Appl. Mater. Interfaces*, 2013, **5**, 1460-1467.

26 T. Ishizaki, Y. Masuda and M. Sakamoto, *Langmuir*, 2011, **27**, 2375-2381.

27 M. L. Zheludkevich, K. A. Yasakau, S. K. Poznyak and M. G. S. Ferreira, *Corros. Sci.*, 2005, **47**, 3368-3383.

28 D. Raps, T. Hack, J. Wehr, M. L. Zheludkevich, A. C. Bastos, M. G. S. Ferreira and O. Nuyken, *Corros. Sci.*, 2009, **51**, 1012-1021.

29 D. Borisova, H. Möhwald and D. G. Shchukin, *ACS Nano*, 2011, **5**, 1939-1946.

30 D. Borisova, D. Akçakayıran, M. Schenderlein, H. Möhwald and D. G. Shchukin, *Adv. Funct. Mater.*, 2013, **23**, 3799-3812.

31 D. G. Shchukin and H. Möhwald, *Small*, 2007, **3**, 926-943.

32 M. J. Hollamby, D. Fix, I. Dönch, D. Borisova, H. Möhwald and D. Shchukin, *Adv. Mater.*, 2011, **23**, 1361-1365.

33 M. F. Haase, D. O. Grigoriev, H. Möhwald and D. G. Shchukin, *Adv. Mater.*, 2012, **24**, 2429-2435.

34 Z. Zheng, X. Huang, M. Schenderlein, D. Borisova, R. Cao, H. Möhwald and D. Shchukin, *Adv. Funct. Mater.*, 2013, **23**, 3307-3314.

35 E. V. Skorb, D. Fix, D. V. Andreeva, H. Möhwald and D. G. Shchukin, *Adv. Funct. Mater.*, 2009, **19**, 2373-2379.

36 Y. Li, L. Li and J. Sun, *Angew. Chem. Int. Ed.*, 2010, **49**, 6129-6133.

37 T. Darmanin, E. Taffin de Givenchy, S. Amigoni and F. Guittard, *Adv. Mater.*, 2013, **25**, 1378-1394.

38 L. K. Wu, J. M. Hu, J. Q. Zhang and C. N. Cao, *Electrochem. Commun.*, 2013, **26**, 85-88.

39 L. K. Wu, J. M. Hu and J. Q. Zhang, *J. Mater. Chem. A*, 2013, **1**, 14471-14475.

40 D.Q. Zhu and W. J. van Ooij, *Electrochim. Acta*, 2004, **49**, 1113-1125.

41 A. Franquet, H. Terryn and J. Vereecken, *Surf. Interface Anal.*, 2004, **36**, 681-684.

42 J. M. Sánchez Amaya, G. Blanco, F. J. Garcia Garcia, M. Bethencourt and F. J. Botana, *Surf. Coat. Technol.*, 2012, **213**, 105-116.

43 A. M. Cabral, W. Trabelsi, R. Serra, M. F. Montemor, M. L. Zheludkevich and M. G. S. Ferreira, *Corros. Sci.*, 2006, **48**, 3740-3758.

44 B. Valdez, S. Kiyota, M. Stoytcheva, R. Zlatev and J. M. Bastidas, *Corros. Sci.*, 2014, **87**, 141-149.

45 J. Hu, X. H. Zhao, S. W. Tang, W. C. Ren and Z. Y. Zhang, *Appl. Surf. Sci.*, 2007, **253**, 8879-8884.

46 M. F. Montemor, A. M. Simões and M. J. Carmezim, *Appl. Surf. Sci.*, 2007, **253**, 6922-6931.

47 M. F. Montemor, R. Pinto and M. G. S. Ferreira, *Electrochim. Acta*, 2009, **54**, 5179-5189.

48 M. L. Zheludkevich, R. Serra, M. F. Montemor, K. A. Yasakau, I. M. M. Salvado and M. G. S. Ferreira, *Electrochim. Acta*, 2005, **51**, 208-217.

49 K. Aramaki, *Corros. Sci.*, 2006, **48**, 766-782.

50 D. Fix, D. V. Andreeva, Y. M. Lvov, D. G. Shchukin and H. Mohwald, *Adv. Funct. Mater.*, 2009, **19**, 1720-1727.

51 J. Wang, L. K. Wu, J. H. Zhou, J. M. Hu, J. Q. Zhang and C.-N. Cao, *Corros. Sci.*, 2013, **68**, 57-65.

Supporting Information

Electrochemically generated sol-gel films as the inhibitor containers of

superhydrophobic surface for active corrosion protection of metals

Xue-Fen Zhang, Rui-Jiao Chen, Yan-Hua Liu, Ji-Ming Hu*

Table S1. The elements content in Ce-incorporated superhydrophobic silica film.

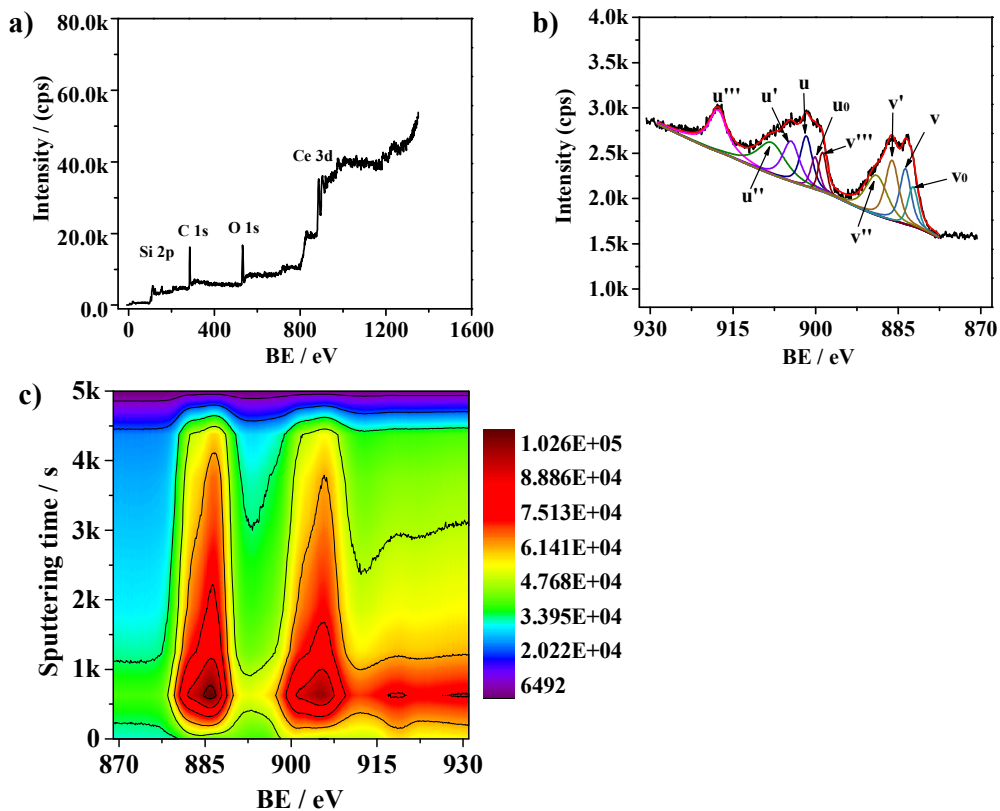| Elt.	Line	Intensity (c/s)	Atomic %	Atomic Ratio	Conc	Units	Error 2-sig	
O	Ka	399.75	61.263	1.0000	34.281	wt.%	1.114	
Si	Ka	711.13	30.772	0.5023	30.226	wt.%	0.742	
Zr	La	40.37	2.068	0.0338	6.597	wt.%	0.952	
Ce	La	66.88	5.897	0.0963	28.896	wt.%	2.603	
			100.000		100.000	wt.%		Total

Fig. S1 XPS spectra of Ce-incorporated superhydrophobic silica film coated on Al

alloy (a) and the enlarged XPS spectrum of Ce 3d (b). (c) Intensity evolution of XPS

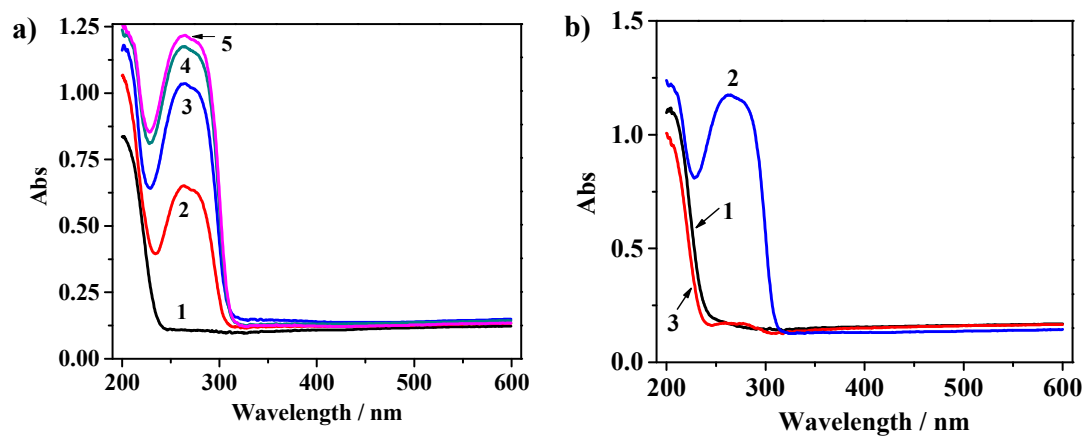spectra of Ce-incorporated superhydrophobic film over the sputtering time.

3

Fig. S2 (a) The UV-Vis absorbance intensity of SiO_2-coated substrates after immersion for 300 s in BTA/EtOH solution with the BTA concentration of 0 (1), 2 (2), 6 (3), 10 (4), and 20 (5) g/L. (b) The UV-Vis absorbance intensity of bare silica film (1), SiO_2-coated substrates after immersion in BTA/EtOH (10 g/L) for 300 s before (2) and after (3) further immersion in DTMS precursor solution for 300 s.
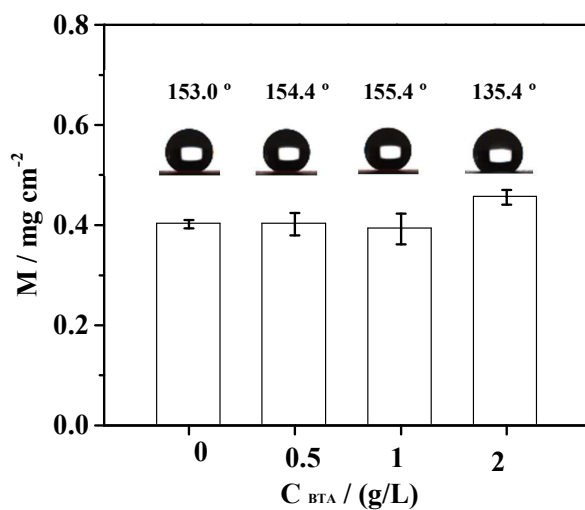
Fig. S3 Dependence of weight of BTA-incorporated superhydrophobic SiO_2 films on

BTA concentration in the mixture precursor. The films are electrodeposited at -1.3

$V/_{Ag/AgCl}$ for 300 s on Al alloy. Optical images of water droplet and the contact angles

are also given.